Micromechanical modeling of the cyclic softening of EUROFER 97 steel

M.F. Giordana, Pierre-François Giroux, Iris Alvarez-Armas, Maxime Sauzay, A. Armas

Available online at www.sciencedirect.com

ScienceDirect

Procedia Engineering 10 (2011) 1268–1273

Engineering Procedia

ICM11

Micromechanical modeling of the cyclic softening of EUROFER 97 steel

M.F. Giordana[a*], P.-F. Giroux[b,c], I. Alvarez-Armas[a], M. Sauzay[b], A. Armas[a]

[a]*Instituto de Física Rosario, CONICET-UNR, Bv. 27 de Febrero 210 Bis, 2000 Rosario, Argentina*
[b]*Commissariat à l'Énergie Atomique, DEN/DANS/DMN/SRMA, 91191 Gif-sur-Yvette Cedex, France*
[c]*Centre des Matériaux / MINES ParisTech, CNRS UMR 7633, B.P. 87, 91003 Évry Cedex, France*

Abstract

The quenched and tempered reduced-activation ferritic/martensitic steel EUROFER 97 is one of the candidates for structural components of fusion reactors. The cyclic behaviour of this steel during isothermal plastic strain-controlled tests is investigated at room temperature. Under Low-Cycle Fatigue (LCF) tests this steel shows, after the first few cycles, a pronounced cyclic softening accompanied by microstructural changes such as the decrease of the dislocation density inside the subgrain and the vanishing of low-angle boundaries. Based on the identified mechanisms of softening a mean-field polycrystalline model is proposed.

Keywords: Martensitic steels; Cyclic softening; Microstructural evolution; Modeling.

1. Introduction

The fast decay characteristics of induced radioactivity imposed on candidate steels of fusion reactors have led to the development of the reduced activation ferritic/martensitic (RAFM) steels. The 9 and 12% Cr transformable steels with low carbon (0.1% max) content and additions of Mo, W, V, Nb, N and other elements, possess high creep-rupture strengths combined with good oxidation and corrosion resistance at elevated temperatures [1]. Although pronounced ageing do not produce marked changes in the tempered martensite lath structure of the steels [2], it is evident from previous results [3] that continuous cycling produces changes in the microstructure and a marked cyclic softening. This effect could become a significant engineering problem affecting creep, swelling and segregation phenomena during irradiation.

Recently, a micromechanical model has been proposed for predicting both the microstructure evolution and the macroscopic softening of a quite similar material [4]. This model based on the well-known Kröner homogenization model [5] is suitable for elastic-plastic constitutive laws. The Kroner model uses the

* Corresponding author. Tel.: +54-0341-4808545.
E-mail address: giordana@ifir-conicet.gov.ar.

1877–7058 © 2011 Published by Elsevier Ltd.
doi:10.1016/j.proeng.2011.04.211

formulation of the so-called “self-consistent scheme”: referring to the problem of an inclusion within an infinite matrix, each grain of a polycrystal is, according to his scheme, successively regarded as an inclusion within the matrix of all other grains: the behaviour of the polycrystal is then calculated by an average process over all grains. This model is relevant for predicting the mechanical behaviour at room temperature, for which no influence of the strain rate is observed.

2. Experimental

2.1. Material and experimental procedures

The material use in this study is EUROFER 97. The final applied heat treatment is austenitizing at 980ºC for 30 min, followed by air cooling and tempering at 760ºC for 90 min, and subsequent air cooling. The chemical composition of the steel in wt% is: 0.12C; 8.93Cr; 0.022Ni; 0.015Mo; 0.2V; 0.001Nb; 0.06Si; 0.47Mn; 0.14Ta; <0.001B; 1.08W; 0.018N and Fe bal.

Low-cycle fatigue tests have been performed using an electromechanical INSTRON testing machine, operating under plastic strain control. Cylindrical specimens are tested in air at room temperature with plastic strain ranges $\Delta\varepsilon_p$=0.2, 0.3, 0.6%. The total strain rate is $\dot{\varepsilon} = 2x10^{-3}\,s^{-1}$. Samples are examined by transmission electron microscopy (TEM) using a Philips EM 300 microscope operating at 100 kV. Several scales are involved in the EUROFER 97 structure [6], prior austenitic grains, packets of blocks, blocks of laths, martensitic laths and subgrains, Fig 1(b). Furthermore, as can be seen in Fig. 1(a), the structure is composed mainly of sub micrometric equiaxed subgrains.

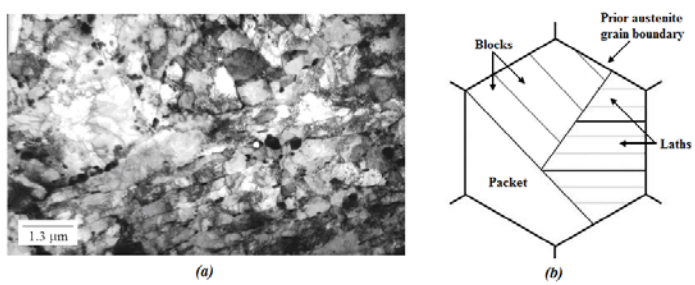

Fig. 1. (a) Tempered martensite structure of the as-received samples after normalization and tempering treatment and (b) schematic microstructure [7]

2.2. Results

Fig. 2 shows the cyclic softening behaviour commonly observed in EUROFER 97 fatigued at room temperature using three different plastic strain ranges 0.2%, 0.3% and 0.6%. As can be seen in Fig. 2 the peak tensile stress of each hysteresis loop shows a continuous softening up to fracture, which is much more pronounced at the beginning of the fatigue life. The maximum peak tensile stress for each curve was measured during the first cycles. After this very short consolidation phase, the cyclic stress amplitude decreases rapidly. The highest quasi-saturation stress level is reached for the highest plastic strain range in a lower number of cycles. All the curves present quite similar behaviour, that is, a transitional stage corresponding to the first part of the fatigue life followed by an almost linear second stage (in a semi-log scale). The first stage depends on the plastic strain range being shorter for the higher plastic strain range.

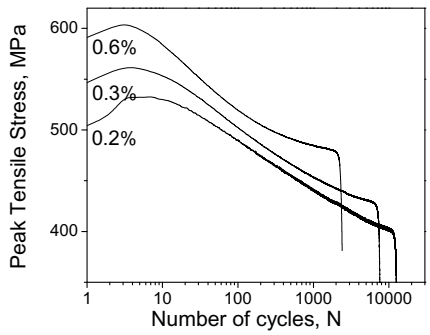

Fig. 2. Cyclic softening curves obtained at RT using three different plastic strain ranges

Cycling at room temperature induces two main microstructural evolutions [8]. First and the most evident, the dislocation density decreases during cycling. Second, some low-angle boundaries (LABs) disappear during cycling. Additional information about the relationship between the cyclic softening and the microstructure evolution, in the same or similar materials, is possible to find in the literature [9, 10].

3.1. Description of the model

A simple mean-field model based on crystalline elastoplasticity is applied in order to predict the polycrystalline Cyclic Strain Stress Curves (CSSCs). The crystallographic structure is supposed to be body-centred cubic (BCC). Therefore, two families of slip systems are considered, {110} and {112} slip planes and <111> slip directions, which all together represent 24 slip systems. Simulations are carried out considering a polycrystal composed of 50 crystals, or martensite blocks, with randomly distributed orientations. Based on the Kröner model, the localization rule is given by the interaction law as follows,

$$\sigma = \Sigma + 2\mu(1-\beta)\left(E^p - \varepsilon^p\right) \qquad \text{with} \quad \beta = \frac{2(4-5\nu)}{15(1-\nu)} \tag{1}$$

Here, σ and Σ are respectively the local (i.e. in the considered block) and macroscopic stress tensors; and ε^p and E^p are the local and macroscopic plastic strain tensors; μ is the shear modulus and ν is the Poisson's ratio, in this case it is considered that $\mu = 82$ GPa , $\nu = 0.3$. The grains are assumed to obey to isotropic elasticity. The Kröner localization rule uses the macroscopic elastic moduli for describing the grain matrix interaction. This model gives reasonable results for low plastic strain, and the macroscopic stress is overestimated by less than 15% for macroscopic plastic strain amplitude of 0.2% [11]. Kroner model is also relevant for predicting the mechanical behaviour at room temperature, for which no influence of the strain rate is observed.

A similar model has been used by Giroux et al. [4], for predicting cyclic softening at high temperature. Therefore, some extra considerations should be taken into account. Sauzay's model [12] is able to predict the decrease in average subboundary misorientation angle in the material during deformation. Following the dislocation dynamics computations of Holec and Dlouhy [13], when the misorientation angle is lower than a critical value, interaction forces between LAB dislocations and the $M_{23}C_6$ precipitates are too weak to preserve LAB stability under stress loading. This leads to the disappearance of the low-angle boundary. Taking into account the LAB precipitate feature of tempered martensitic/ferritic steels, the critical misorientation angle is about 0.4º [13]. Considering the proportion of vanished low-angle boundaries [14], an estimation of subgrain growth is computed by Giroux et al for tensile deformation [14].

3.1.1. Backstress - Bowing out of a dislocation

As can be seen in the as-received material, there are many dislocations pinned up on LABs. Under stresses, those dislocations start bowing out. Fig. 3(a) shows a schematic representation. During one cycle, the evolution of the local backstress on each slip system is computed based on a simple tension line model in dislocation microstructures [15, 16].

Based on Fig. 3(a) it is possible to deduce a relationship between the plastic slip and the radius of curvature of the dislocation $\left(\gamma = \gamma_{(R)}\right)$ in the following way. The plastic slip on slip system *i* is expressed by the Orowan's law:

$$\gamma^i = \left(\rho_e^i + \rho_s^i\right) l b \tag{2}$$

With *l* defined as the slipping area divided by the subgrain size (*d*), Fig. 3(a), and *b* is the Burgers vector ($\mathrm{b} = 2.54\times10^{-10}\,\mathrm{m}$). After computing this length, Eq. 3 is:

$$\gamma^i = \frac{\left(\rho_e^i + \rho_s^i\right) b}{d}\left[R^2 \operatorname{arctg}\left(4\frac{R^2}{d^2} - 1\right)^{-1/2} - \frac{d}{4}\left(4R^2 - d^2\right)^{1/2}\right] \tag{3}$$

In this equation *R* is the curvature radius of the dislocation depending on the local shear stress.

Taking into account the tension line model, the backstress on slip system *i* $\left(x^i = x^i{}_{(R)}\right)$ as a function of the curvature radius is expressed as follows [17]:

$$x^i = \frac{T}{Rb} = \frac{\mu b}{2R} \tag{4}$$

With T the tension line. As known, the tension line is not the same for edge and screw dislocations [15], however, for the sake of simplicity an average value is used ($T \approx 1/2\,\mu b^2$). Relating the plastic slip and the backstress through the radius of curvature, the following equation is obtained, presented here in the differential form:

$$\dot{x}^i = \frac{2d\left(x^i\right)^3\left(\dot{\gamma}_e^i + \dot{\gamma}_s^i\right)}{\left(\rho_e^i + \rho_s^i\right) b^3 \mu^2}\left\{\frac{1}{2}\left[\frac{\mu^2 b^2}{\left(x^i\right)^2 d^2} - 1\right]^{-1/2} - \arctan\left[\frac{\mu^2 b^2}{\left(x^i\right)^2 d^2} - 1\right]^{-1/2}\right\}^{-1} \tag{5}$$

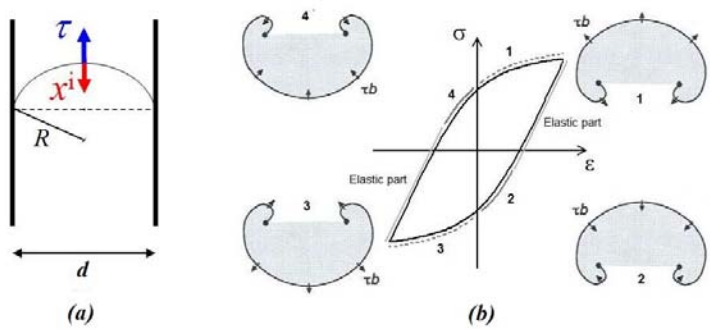

Fig. 3. (a) Bowing out of a dislocation which is pinned up on LABs; (b) Analogous activation of Frank-Read sources during cycling

3.1.2. Dislocation density evolution

In this section, the evolution of the dislocation density as a function of the plastic slip (γ) is evaluated. First, the rate of production of dislocations during cycling is determined, and then the rate of annihilation of dislocations for an increment of plastic slip $d\gamma$. To study the production of dislocations, the Frank-Read source activation during four different steps is considered. Fig. 3(b) shows an hysteresis loop divided into six parts, two of them are the elastic parts, in which dislocations are motionless. Parts 1 and 4 are in tension, and 2 and 3 are in compression.

During part 1, it the usual activation of the Frank-Read sources taking place and the rate of production of edge dislocations could be written as follows [18]:

$$d\rho_{e,i}^{+} = \frac{2}{bd} d\gamma_{s,i} \tag{6}$$

With $d\rho_{e,i}^{+}$ the production increment of edge dislocation density due to an increment of screw plastic slip $d\gamma_{s,i}$. During part 2, it is considered that the dislocations come back to the source, annihilating one another. The equation to describe that event is the same as Eq. 6 but with a minus sign in the right hand term. Parts 3 and 4 are described in the same way as parts 1 and 2, even when the bowing out of the dislocation occurs in the opposite direction. The rate of annihilation of dislocations, for the four different parts, was expressed by Essmann and Mughrabi [18] in the following way,

$$d\rho_{e,i}^{-} = 2\frac{y_e}{b}\rho_{e,i}\left|d\gamma_{e,i}\right| \tag{7}$$

With y_e the athermal edge annihilation distance [18], in this case it is considered that $y_e = 3nm$ ($y_s = 50nm$). So, for the total evolution of edge dislocation density it is obtained,

$$d\rho_{e,i} = d\rho_{e,i}^{+} - d\rho_{e,i}^{-} = \frac{2}{bd} d\gamma_{s,i} - 2\frac{y_e}{b}\rho_{e,i}\left|d\gamma_{e,i}\right| \tag{8}$$

The evolution of screw dislocation density could be described similarly.

3.2. Results and discussion

Viscoplastic flow law parameters were adjusted in order to minimize the strain rate effect. Block behaviour could therefore be considered as elastic-plastic in agreement with test results. Some of the parameter values that are used in the model are the followings: $\rho = 2.6\times10^{14}\mathrm{m}^{-2}$, $\theta_0 = 1.7°$, $d_0 = 0.7\mu m$, these values were estimated from experimental observations. In order to adjust the activation volume and energy, tensile tests, using a plastic strain range of 0.6%, have been simulated. These two parameters have been chosen in such way that the strain rate effect is negligible in agreement with experimental test results at room temperature. Another adjustable parameter is τ_0 [4], instead of taking τ_0 equal to zero as it was done by Giroux, this parameter has been adjusted in order to reproduce, as best as possible, the first quarter of the first cycle. At room temperature, the solid solution and precipitate effects are no longer negligible.

So, the optimization of the parameters is carried out using only the first loop at a plastic strain range of 0.6%. Therefore, in order to validate the proposed model, tests using plastic strain ranges 0.2% and 0.3% are simulated and compared to experimental data. Fig. 4 shows the results of the model for the first cycle of each case. Although only three parameters are adjusted, the model shows good agreement with experimental stress-strain curves. The next step of this work is to apply many cycles for predicting the cyclic softening and the microstructure evolution.

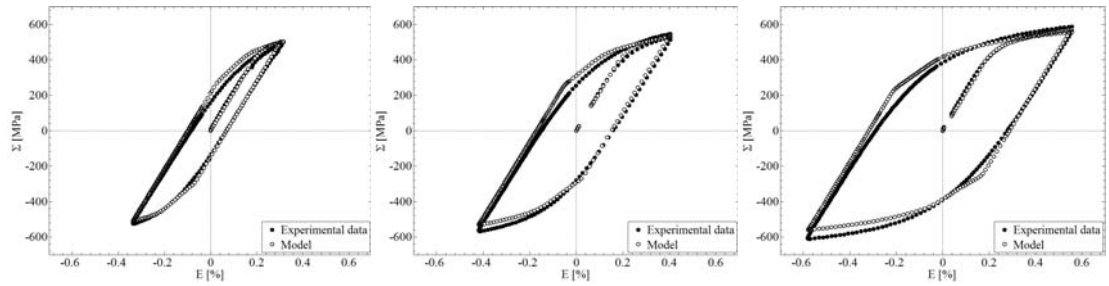

Fig. 4. Comparison between experiment and simulation: first stress-strain loops using plastic strain ranges of (a) 0.2%; (b) 0.3% and (c) 0.6%

4. Conclusions

Low-cycle fatigue tests using three different plastic strain ranges (0.2 %, 0.3% and 0.6%) are carried out at room temperature on EUROFER 97 steel. Experimental results show a pronounced cyclic softening, which is accompanied by microstructural changes.

The model gives reasonable predictions at the first cycle. However, work is in progress in order to base the model on the well-known Hill-Hutchinson mean-field homogenization model [19, 20]. Rachdi and Sauzay [11] show that the HH model overestimate the macroscopic stress by less than 6%, even for macroscopic plastic strain amplitude of 1%. Anyway, no significant difference is expected at low plastic strain.

References

[1] Klueh RL, Harries DR. ASTM Mono3, West Conshohocken, PA (USA), 2001.
[2] Jones W, Hills CR, Polonis DH. Metall Trans 1991;22A:1049.
[3] Armas AF, Petersen C, Schmitt R, Avalos M, Alvarez I. J Nucl Mater 2004;329–333:252.
[4] Giroux PF, Dalle F, Sauzay M, Caës C, Fournier B, Morgeneyer T, Gourgues-Lorenzon AF. Proc Eng 2 2010;2141.
[5] Kröner E. Acta Metall 1961; 9:155.
[6] Marder JM, Marder AR. Trans ASME 1969;62:1.
[7] Kitahara H, Ueji R, Tsuji N, Minamino Y, Acta Mater. 2006, 54:1279-1288.
[8] Giordana MF, Alvarez-Armas I, Sauzay M, Armas A. Key Eng. Mat. 2011;465 ;358-361.
[9] Marmy P, Kruml T. J Nucl Mater 2008;377:52-58.
[10] Kunz L, Lukáš P. *European Structural Integrity Society 2002 ,29;* 37-44**.**
[11]Rachdi F, Sauzay M; Congres Francais de Mecanique. Besancon, France, Sept 2011.
[12] Sauzay M., Mater. Sci. Eng. A 2009;510–511;74–80.
[13] Holec D, Dlouhy A, Z. Metallkd. 2005;96–6;558–565.
[14] Giroux P.-F, Dalle F, Sauzay M, Malaplate J, Fournier B, Gourgues-Lorenzon A.F. Mater Sci and Eng A2010;*527; 3984–3993.*
[15] Brown L. Phil Mag 2006;86:4055.
[16] El-Awady J, Ghoniem N, Mughrabi H. TMS 2007.
[17] Hull D. Introduction to Dislocations*.* Pergamon Press. 1965, p. 80.
[18] Essmann U, Mughrabi H. Philos Mag 1979;40:731.
[19] Hill R. J Mech Phys Sol 1965;13:89.
[20] Hutchinson JW. J Mech Phys Sol 1970;319:247.